FLOW SEPARATION OF AXIAL COMPRESSOR CASCADE BLADES

Dr. Arkan Kh. Al-Taie
(Assist. Prof.) Mech. Eng. Dept., UOT
Baghdad - Iraq

Sabah Faleh Habeeb
(M.Sc. Student), Mech. Eng. Dept., UOT
Baghdad - Iraq

ABSTRACT

An experimental and theoretical investigation of the effect of flow separation on the performance of a cascade NACA 65_(12)10 axial compressor blade has been carried out. The experimental work includes the fabrication of three blades from wood, each having a chord (100mm) but one of these blades having a span of (90mm) for smoke tunnel testing and the other two blades having a span of (380mm) for wind tunnel testing.The two blades were connected by suitable mechanism in order to be fixed in the wind tunnel protractor and rotated in the required stagger angle. The cascade was tested in an open type low-speed subsonic (Mach number=0.117) wind tunnel, for Reynolds number (Re=239605) based on maximum velocity (35 m/s) and airfoil chord length. The total and static pressures were measured in selected points between the two blades for stagger angles of (4^0, 0^o,-4^0,-$8^0$and -12^0) by using a multi-tube manometer and a pitot static tube. The small blade (90mm span) is tested in the smoke tunnel to visualize the real behavior of flow separation. The theoretical work includes using the software FLUENT (V6.2) to simulate the flow between the two blades. The study shows that the flow separation begins when the cascade are inclined at a stagger angle of (-4^0) on the suction side of the lower blade at a position (96%chord experimentally and 98%chord theoretically). Then, the separation zone increases with increased stagger angle (in clockwise direction) and reach to the position (61%chord experimentally and 63%chord theoretically) at a stagger angle (-12^0).These results are validated by a smoke tunnel tests.This separation affects the performance of the compressor, where the static pressure ratio (p_{s_e} / p_{s_i}) decreases as the separation zone gets bigger. The range of working stagger angle is then calculated. It was found in the range (-18^0 to 36^0). The flow behavior between the two blades shows that the blade-to-blade configuration works as nozzle-diffuser. The theoretical results were compared with the experimental results and good agreement was obtained.

الخلاصة:

تم في هذا البحث اجراء دراسة عملية ونظرية لتاثير انفصال الجريان على اداء الريشتين المتعاقبتين للضاغطة المحورية من نوع [NACA 65_ (12)10] . الجزء العملي يتضمن تصنيع ثلاث ريش من مادة الخشب, وتر كل ريشة (100ملم) لكن احدى الريش ذات عرض(90 ملم) لاختبارات النفق الدخاني والريشتين المتبقتين ذواتا عرض(380ملم)لاختبارات النفق الهوائي. تربط الريشتيين المستخدمتين لاختبارات النفق الهوائي بآليه مناسبة لكي تثتبت بمنقلة النفق وبالتالي يمكن تدويرها بالزاوية المطلوبة. تم اختبار متعاقبة الريشتين في نفق هوائي تحت صوتي واطى السرعة لعدد رينولد(Re=239605) المحسوب على اساس السرعة القصوى (35م\ثا) وطول وتر الريشة. لقد تم قياس الضغط الكلي والضغط الاستاتيكي للنقاط المختاره بين ريشتي الضاغطة لخمس زوايا أنحراف هي (4,0,4-,8- و12-) باستخدام مانوميترمتعدد الانابيب وأنبوب بيتوت-أستاتي. تم أختبار الريشة الصغيرة (ذات عرض90 ملم) بأستخدام النفق الدخاني لرؤية السلوك الحقيقي لأنفصال الجريان. الدراسة النظرية تتضمن استخدام

البرنامج الجاهز (FLUENT V6.2) لمحاكات الجريان بين الريشتين. أظهرت الدراسة بأن الأنفصال يبدأ عندما تكون زاوية الأنحراف (4-) حيث يحدث على السطح العلوي للريشة السفلى وبمسافة (96% من الوتر عمليا" و98 % من الوتر نظريا") من الدخول الى الخروج للمتعاقبة'. وبعد ذلك تزداد منطقة الأنفصال بأزدياد زاوية الأنحراف(stagger angle)(بأتجاه عقرب الساعة) حتى تصل الى (61% من الوتر عمليا" و63% من الوتر نظريا") من الدخول الى الخروج عند زاوية أنحراف (12-) وهذا ما يوضحه أختبار النفق الدخاني. يؤثر الأنفصال على أداء الريشتين المتعاقبتين حيث تقل نسبة الضغط (الضغط الستاتيكي الخارج الى الضغط الستاتيكي الداخل) بأزدياد منطقة الانفصال. وبعد ذلك تم حساب المدى الشغال لزوايا الأنحراف . الذي وجد ضمن المدى (من-18 الى 36) . أن سلوك الجريان بين الريشتين يبين بأن الريشتين المتعاقبتين تعملان كبوق متقارب- متباعد. تمت مقارنة النتائج النظرية مع النتائج العملية وجد تقارب جيد بين تلك النتائج.

KEYWORDS: Axial Compressor Cascade, Viscous Flow, Separation, FLUENT, Visualization

INTRODUCTION:

The compressor, which is the important part of gas turbine engines, has to be given special attention during operation. The main task of the axial-flow compressor is to increase the pressure of air by converting air kinetic energy through a series of rotating and stationary blades. One of the most important problems that affect performance is the flow separation. Separation starts by deviation of fluid particles away from blade surface in the boundary layer. This causes a drop in kinetic energy, and cause the flow to re circulate [You D. AND Moin, P., 2006]. After stall region the fluid particles velocity reaches to zero in boundary layer near to blade surface and this deceleration causes increasing in boundary layer thickness and at a small distance after stall region the particles stop and reverse in direction due to positive pressure gradient. The low Reynolds number in conjunction with the local adverse pressure gradient makes it susceptible to flow separation [Meinhard T. Schobeiri etal, 2003]. This study consists of two major parts: the experimental part a cascade tested in an open jet low speed wind tunnel. The total and static pressure between two axial compressor blades were measured using a Pitot - static tube and a manometer. To visualize the flow a smoke tunnel was used. The stagger angle was taken equals (4^0, 0^0,-4^0,-8^0, and-12^0). Secondary, in the theoretical part that depends on simulation the flow between the two blades by using a software **FLUENT**. The objectives of this paper are:

1. Study the effect of viscous flow separation (through the cascade of an axial compressor) on the flow variables (velocity, static pressure, total pressure…etc) by utilizing FLUENT (V6.2) software.
2. Investigate the effect of stagger angle on flow separation.
3. Comparison of the experimental results with the theoretical results.

THEORITICAL PART:

* Assumptions:

The flow is steady, two-dimensional, incompressible , turbulent, Newtonian, isotropicand isothermal.

* Governing Equations:

The domain for which the model is build is shown in fig.(1) since the flow through a compressor is three-dimensional and quite complex, a simplified approach is adopted to analyze the fluid flow through cascade passage in two dimensions. Figs.(1) and (2) show the cascade and the physical domain. The equations of continuity, momentum and turbulence model are [Hill, P. G., 1965]:

- Continuity Equation:

$$\frac{\partial u}{\partial x}+\frac{\partial v}{\partial y}=0 \qquad \text{(a).}$$

- X-Momentum Equation:

$$\rho\frac{\partial u^2}{\partial x}+\rho\frac{\partial uv}{\partial y}-\frac{\partial}{\partial x}\left[\mu_e\frac{\partial u}{\partial x}\right]-\frac{\partial}{\partial y}\left[\mu_e\frac{\partial u}{\partial y}\right]=-\frac{\partial p}{\partial x}+\frac{\partial}{\partial x}\left[\mu_e\frac{\partial u}{\partial x}\right]+\frac{\partial}{\partial y}\left[\mu_e\frac{\partial v}{\partial x}\right] \quad \text{(b).}$$

- Y-Momentum Equation:

$$\rho\frac{\partial uv}{\partial x}+\rho\frac{\partial v^2}{\partial y}-\frac{\partial}{\partial x}\left[\mu_e\frac{\partial v}{\partial x}\right]-\frac{\partial}{\partial y}\left[\mu_e\frac{\partial v}{\partial y}\right]=-\frac{\partial p}{\partial y}+\frac{\partial}{\partial x}\left[\mu_e\frac{\partial u}{\partial y}\right]+\frac{\partial}{\partial y}\left[\mu_e\frac{\partial v}{\partial y}\right] \quad \text{(c).}$$

- The turbulence kinetic energy – dissipation model at high Reynolds number is used [Moult, A. etal,1977].

A-Turbulence kinetic energy: $K=0.5\left(u'^2+v'^2+w'^2\right)$

$$\rho\left[\frac{\partial Ku}{\partial x}+\frac{\partial Kv}{\partial y}\right]=\frac{\partial}{\partial x}\left[\frac{\mu_e}{\sigma_k}\frac{\partial K}{\partial x}\right]+\frac{\partial}{\partial y}\left[\frac{\mu_e}{\sigma_k}\frac{\partial K}{\partial y}\right]+G_k-\rho\varepsilon \quad \text{(d).}$$

The quantity G_k is the generation term for the kinetic energy of turbulence given by:

$$G_k=\mu_t\left\{2\left[\left(\frac{\partial u}{\partial x}\right)^2+\left(\frac{\partial v}{\partial y}\right)^2+\left(\frac{\partial u}{\partial y}+\frac{\partial v}{\partial x}\right)^2\right]\right\} \quad \text{(e).}$$

B-Dissipation: $\left[\varepsilon=\nu\left(\frac{\partial u'}{\partial y}+\frac{\partial v'}{\partial x}\right)^2\right]$

$$\rho\left[\frac{\partial \varepsilon u}{\partial x}+\frac{\partial \varepsilon v}{\partial y}\right]=\frac{\partial}{\partial x}\left[\frac{\mu_e}{\sigma_\varepsilon}\frac{\partial \varepsilon}{\partial x}\right]+\frac{\partial}{\partial y}\left[\frac{\mu_e}{\sigma_\varepsilon}\frac{\partial \varepsilon}{\partial y}\right]+\left(C_1G_k-C_2\rho\varepsilon\right)\varepsilon/K \quad \text{(f).}$$

The $K-\varepsilon$ turbulence model was extended by ref**.** [Jones, W. P. and Launder, B. E., 1972] to low-Reynolds number flow as follows:

$$\rho\left[\frac{\partial Ku}{\partial x}+\frac{\partial Kv}{\partial y}\right]=\frac{\partial}{\partial x}\left[\left(\frac{\mu_t}{\sigma_k}+\mu\right)\frac{\partial K}{\partial x}\right]+\frac{\partial}{\partial y}\left[\left(\frac{\mu_t}{\sigma_k}+\mu\right)\frac{\partial K}{\partial y}\right]+\mu_t\left[2\left(\frac{\partial u}{\partial x}\right)^2+2\left(\frac{\partial v}{\partial y}\right)^2+\left(\frac{\partial u}{\partial y}+\frac{\partial v}{\partial x}\right)^2\right]-2\mu\left[\frac{\partial K^{0.5}}{\partial x}+\frac{\partial K^{0.5}}{\partial y}\right]^2-\rho\varepsilon \quad \text{(g).}$$

$$\rho\left[\frac{\partial \varepsilon u}{\partial x}+\frac{\partial \varepsilon v}{\partial y}\right]=\frac{\partial}{\partial x}\left[\left(\frac{\mu_t}{\sigma_\varepsilon}+\mu\right)\frac{\partial \varepsilon}{\partial x}\right]+\frac{\partial}{\partial y}\left[\left(\frac{\mu_t}{\sigma_\varepsilon}+\mu\right)\frac{\partial \varepsilon}{\partial y}\right]+\frac{C_1\mu_t}{K}\varepsilon\left[2\left(\frac{\partial u}{\partial x}\right)^2+2\left(\frac{\partial v}{\partial y}\right)^2+\left(\frac{\partial u}{\partial y}+\frac{\partial v}{\partial x}\right)^2\right]-\frac{\rho C_2\varepsilon^2}{K}-2\upsilon\mu_t\left[\frac{\partial^2 u}{\partial x^2}+\frac{\partial^2 u}{\partial x\partial y}+\frac{\partial^2 v}{\partial x\partial y}+\frac{\partial^2 v}{\partial y^2}\right] \quad \text{(h).}$$

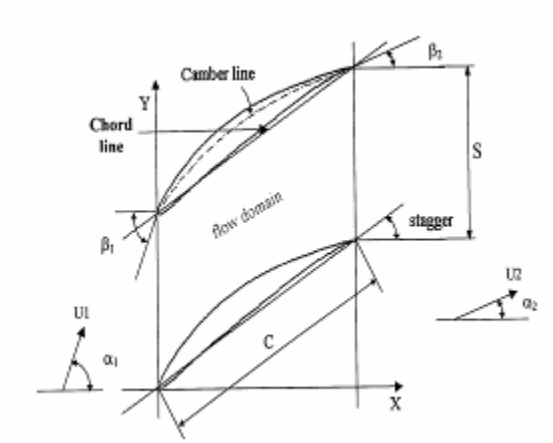

Fig.(1): Compressor Cascade Geometry.

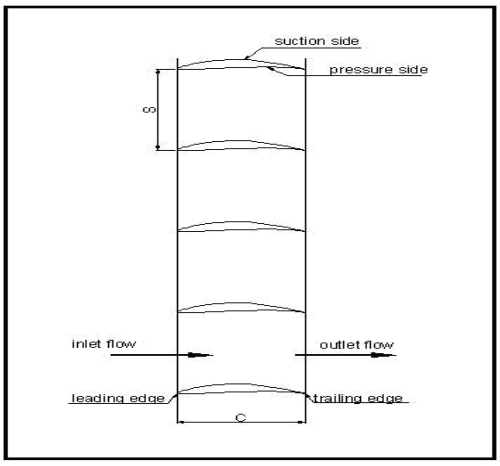

Fig.(2): General View of the Cascade.

*** FLUENT Code:**

- Analysis Steps:

There are two processors used to solve the flow equations:

A. preprocessor is a program that structure creates the geometry and grid by using GAMBIT as follows:

- Modeling of geometry, fig.(3) and fig.(4).
- Mesh generation (Discitization), fig.(5).
- Boundary conditions. There are three type of boundary conditions:

a. Inlet boundary conditions(velocity and pressure inlet).
b. Outlet flow boundary conditions.
c. Solid surface(wall) boundary conditions.
d. Periodic boundary condition(flow regions before and after two blades).

B. Postprocessor: is:

- Solving Navier-Stokes equations (which includes continuity and momentum equations) as wall as turbulent flow model by using FLUENT software with ().

- Plotting the results.

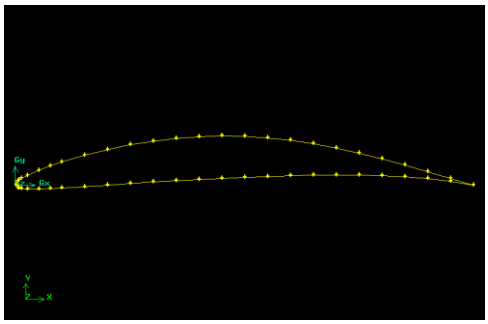

Fig.(3):Axial compressor Blade by Points and Edges.

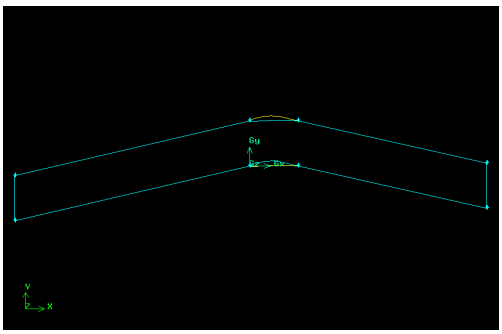

Fig.(4):Axial Compressor Blade as a face.

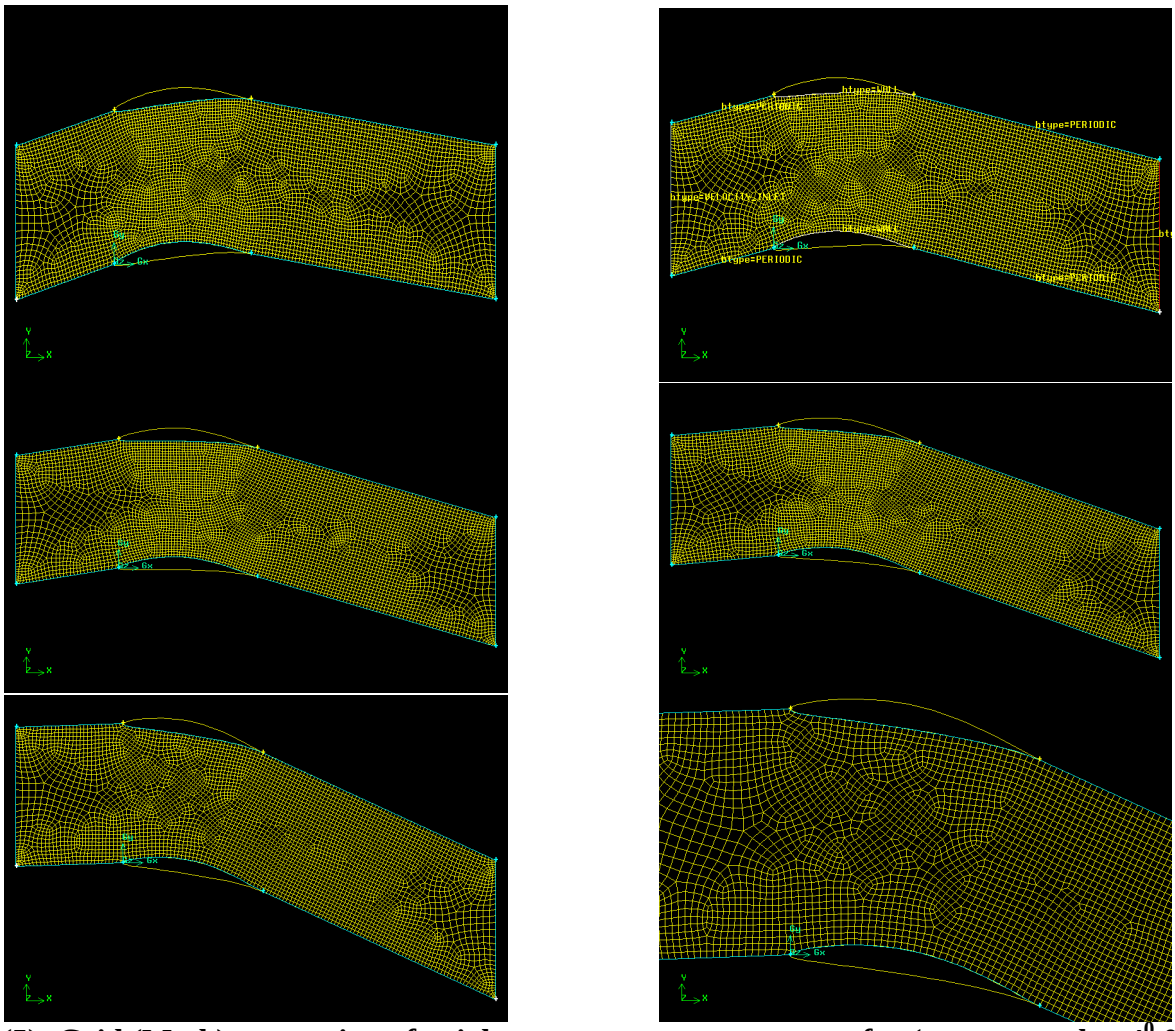

Fig. (5): Grid (Mesh) generation of axial compressor vanes passage for (stagger angle =4^0,0^0,-4^0,-8^0 and -12^0).

EXPERIMENTAL WORK:

*** Blade to Blade Configuration:**

In the present work a cascade consists of two blades, each having a chord of (100mm) but one of these blades has a span of (90mm) and the other two blades have a span of (380mm) were made from wood fig.(6). The two blades of (380mm in span) are connected by suitable mechanism, as shown in fig.(7) in order to be fixed in wind tunnel protractor and achieved on required stagger angle. The two blates are fixed by aluminum plates, fig.(7).

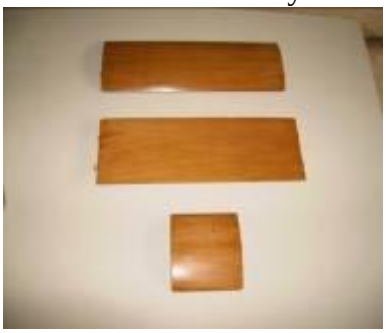

Fig.(6): Axial Compressor Blades NACA 65_ (12)10.

Fig.(7): Blade to Blade Configuration.

*** Apparatus:**

- Subsonic Wind Tunnel:

Low- speed subsonic (Mach number=0.117) open type wind tunnel is used in this work of cross section of (305mm* 305mm). Wind speed of (35m/s) is achievable allowing experiments on many aspects of incompressible air flow and subsonic aerodynamics to be performed at satisfactory Reynolds number. Reynolds number is (Re=239605) based on inlet velocity and blade chord. The tunnel has a smooth contraction fitted with the protective screen. The test section is constructed of clear Perspex, to see the blade to blade configuration clearly with a square cross section of (305mm×305mm) and a length of (610mm). The blade to blade configuration was put inside the test section parallel to flow direction and connect by protractor to limit stagger angle. The control of the stagger angle of the blade to blade configuration was made by a suitable mechanism, fig.(9). The upper surface of the test section has a slot used to fix the pitot-static tube to measure the static pressure and total pressure. Fig.(8) is a photo of the wind tunnel and the working section. Downstream of the test section is a diffuser which leads to an axial flow fan driven by a (5.6kW three phase A.C motor). The flow is controlled by a butterfly valve before exhaust to atmosphere through exhaust section. The air enters the tunnel through a carefully shaped diffuser. The test section gives a full visibility of flow field.

Fig.(8): Wind Tunnel Device (Open Circuit) and Multi-Tube Manometer.

Fig.(9): Protractor of Subsonic Low Speed Wind Tunnel.

- Multi Tube Manometer:

A water multi tube manometer was used to measure total and static pressure between the two axial flow compressor blades, fig.(10). The manometer holes are connected to the Pitot - static tube by suitable connection pipes.

- Pitot – Static Tube:

The purpose of using pitot – static tube is to measure air static pressure, total pressure and then velocity inside test section. The external dimensions are (5mm) diameter, (200mm) arm length. Tube reading were corrected according to reference [Omran, K. J.,2003] as following:

$$\Delta p = p_d = p_t - p_s = \rho_{water} * g * \Delta H_{water} \quad \text{(i).}$$

$$p_d = \frac{1}{2} * E * \rho_{air} * U^2{}_{\infty} \quad \text{(j).}$$

$$\Delta p = \rho_{water} * g * \Delta H_{water} = \frac{1}{2} * E * \rho_{air} * U^2 \quad \text{(k).}$$

$$E = E_0 + \omega + \Omega \quad \text{(l).}$$

Where: E=Correction coefficient, ω =Viscosity coefficients, its value(0), Ω =Effect of distance from tube to wall which is found from fig.(11), E_0 =Effect of static pressure holes distance of (0.9976) value.

Fig.(10): Multi Tube Manometer.

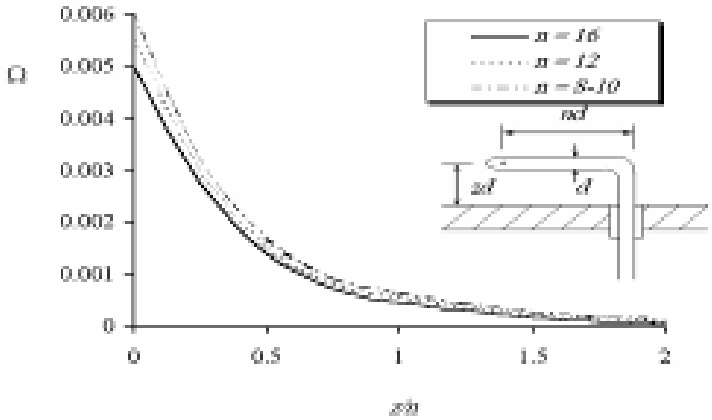

Fig.(11): Correction of Pitot - static tube Distance. [Omran, K. J., 2003].

Smoke Tunnel:

To illustrate a real view of flow development and separation, a smoke tunnel was used as shown in fig.(12). The air is drawn by a fan which is rotated by an electrical motor of variable velocity at the top of the tunnel. The air enters to the tunnel at the base. The test section has dimensions of (180mm) width, (240mm) height and (100mm) deep. The models installed in the back wall of the test section, the front wall of the test section are easy to remove. It is made of clear Perspex. Smoke generation is controlled at the bottom of the tunnel. The section has (23) holes from it smoke enter. The space between any two adjacent holes is (7mm). A high light source is put in the sides of the test section to see smoke clearly. The smoke generated by a smoke generator which evaporates kerosene in class evaporator carried on the front wall of the smoke generator. The smoke generated is dragged by the fan at the top of the tunnel through the test section. Flow Photo is taken using a digital Camera.

Fig.(12): Smoke Tunnel.

*** Procedure of Experiments:**

The flow between two axial flow compressor blades was tested by wind tunnel as described in the following steps:

- Measure the atmospheric pressure and temperature before carrying out the experiments to calculate the air density accurately.
- Fix the blade to blade configuration in the test section with the required stagger angle.
- Prepare the multi tube manometer, controlling speed valve, and pitot static tube.

- Operating the wind tunnel for (15min) to reach steady state conditions.
- Reading the dynamic head by using pitot static-tube which is connected to multi tube manometer by suitable connection tubes.
- Repeating the previous procedure for other stagger angles ranges from(4^0 to -12^0).
- The experiments carried out in smoke tunnel were as following:
- Fill the bottle with Kerosene to the required limit.
- Put the model inside smoke tunnel test section and fixed at a certain angle indicated by protractor.
- 3. Turn on the smoke generator.
- 4. After about (3minutes) the smoke begins to formulate.
- 5. After smoke formulation the fan is turned on and controlled by the speed controller.
- 6. A high resolution digital camera was then used to photograph the models and flow.

RESULTS AND DISCUSION:

* Experimental Results:

The experimental results are presented for three different curve lines located at (0.125,0.5 and 0.875) of (S) as shown in fig.(13). The operating and boundary conditions of the blades and flow passage are listed in table(1).

Table (1): Operating and Boundary Conditions.

Case	Stagger Angle in (degree)	Inlet Velocity (m/s)	Number of grid points	Static Pressure Ratio
1	4	35	63	1.08
2	0	35	63	1.12
3	-4	35	63	1.1
4	-8	35	63	1.07
5	-12	35	63	1.04

The velocity and static pressure distribution (for the three sections) of flow between the two blades for stagger angle (4^0, 0^0,-4^0, -8^0 and -12^0) are presented in fig.(14)and(15). These figures show that the flow is accelerated along section 1 (0.125S) up to a certain position,(refer to third column of table(2). Then the flow decelerates to the exit for stagger angles (4^0 and 0^0) up to a certain position, see the fourth column of table (2) for stagger angles (-4^0, -8^0 and-12^0) where the flow is separated. The flow decelerates along section 3 (0.875S) from the inlet to the exit for all taken stagger angles. The velocity and static pressure remains constant along the section 2(0.5S) from the inlet to the exit for stagger angles (-8^0 and -12^0) and to a certain position for stagger angles (4^0, 0^0 and -4^0), the fifth column of table (2). Then the flow decelerates to the exit. The pressure ratio is the exit static pressure from blade to blade passage divided by inlet static pressure. The pressure ratio for all cases is shown in table (2).

The reason behind such behavior is the effect of stagger angle. Within a certain range of stagger angles (from 4^0 to -4^0) the flow remains in contact with the blade surface. As the stagger angle is increased, the blade profile forces the flow a way from its surface, hence, the flow starts to separate. Separation starts close to the trailing edge and progresses upwards as the stagger angle is changed (from -4^0 to -12^0). This effect is not clear in the middle section of the passage as the profile effects on flow behavior diminishes. The behavior of static pressure distribution is complimentary to the behavior of velocity. The flow separate from the suction side of the lower blade of cascade for stagger angle (from -4^0 to -12^0) because of adverse pressure gradient.

Table (2): Experimental properties and behavior of flow between two blades in wind tunnel.

Case	Stagger angles in (degrees)	Location of maximum velocity and minimum static pressure along section 1 (%chord)	Location of separation point along section 1 (%chord)	Location of flow deceleration along section 2 (%chord)	Pressure ratio
1	4	43	-	87.3	1.08
2	0	37.5	-	75	1.12
3	-4	36	96	73	1.1
4	-8	25	64	-	1.07
5	-12	12	61	-	1.04

The total pressure distribution of flow between two axial compressor blades for different stagger angle is presented in figure (16) .This figure show that the fluid total pressure decreases as it passage from the inlet to the exit due to friction losses. The total pressure losses increases when the stagger angle increases (in clockwise direction) and the maximum total pressure losses occurs for stagger angle (-12^0) in separation region.

Figure (17) presents the pressure ratio distribution for stagger angles (4^0, 0^0,-4^0, -8^0 and -12^0). The pressure ratio decreases when the stagger angle increases and separation zone increases, see table (2). By using curve fitting method for this polynomial distribution, the concluded mathematical relationship between this pressure ratio and stagger angle for NACA 65_(12)10 axial compressor cascade is:

$$\frac{p_{s_e}}{p_{s_i}} = 1.1057 - 0.0021\theta - 0.0007\theta^2 \qquad \text{(m).}$$

Where: θ: Stagger angle in (degrees). $\frac{p_{s_e}}{p_{s_i}}$: Pressure ratio.

By equating equation (m) to one, the range of stagger angle for NACA 65_(12) 10 axial compressor blade aerofoil is (from -18^0 to 36^0).

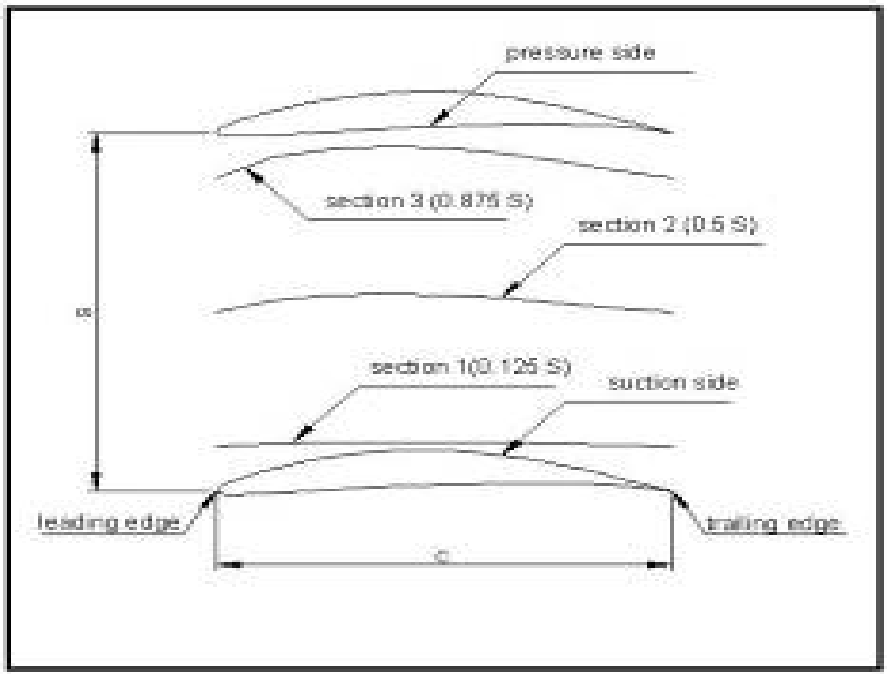

Fig.(13): Blade to blade configuration with taken three sections in flow passage.

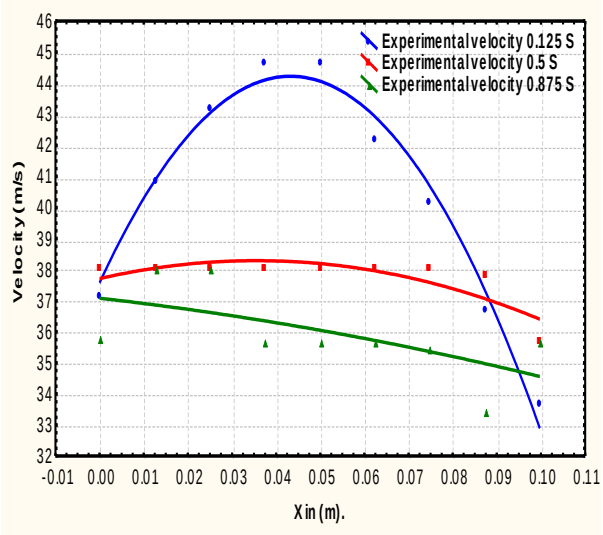

(a) For stagger angle (4^0).

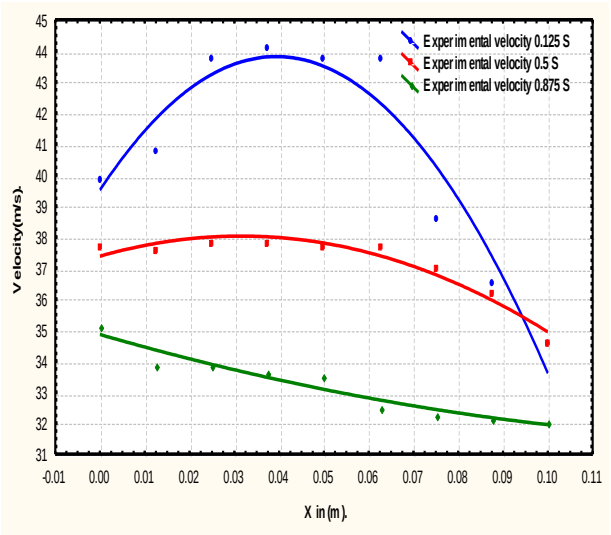

(b) For stagger angle (0^0).

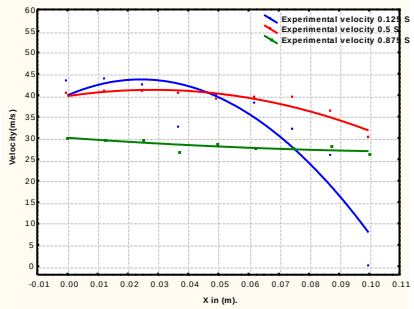

(c) For stagger angle=-4.

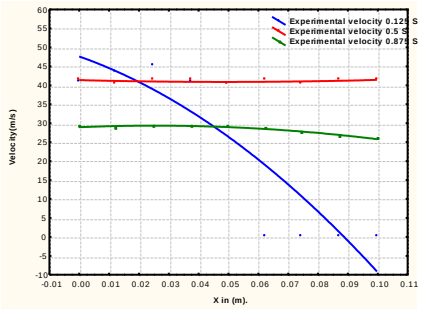

(d) For stagger angle=-8.

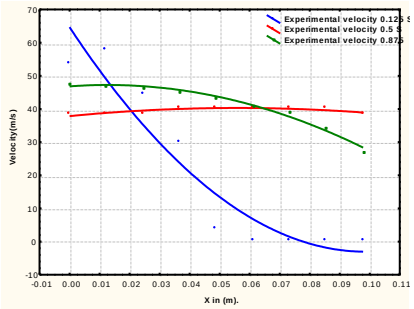

(e) For stagger angle=-12.

Fig.(14): Velocity distribution for (0.125S, 0.5S and 0.875S).

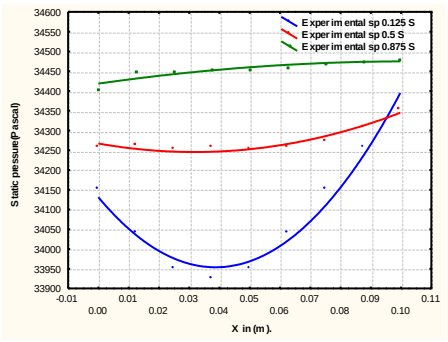

(a) For stagger angle=4.

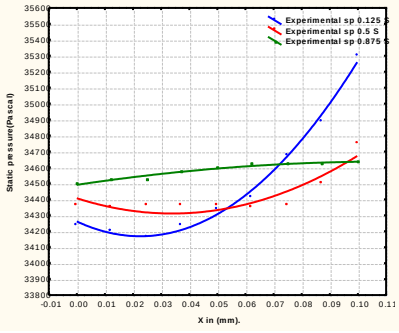

(b) For stagger angle=0.

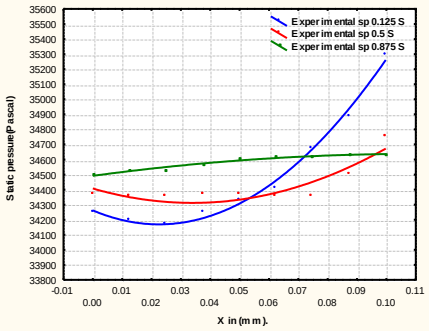

(c) For stagger angle=-4

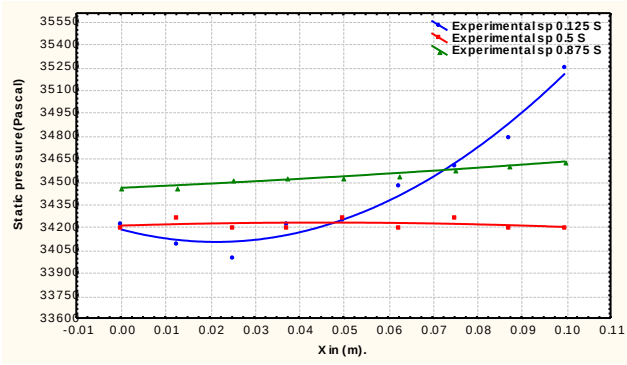

(d) For stagger angle=-8.

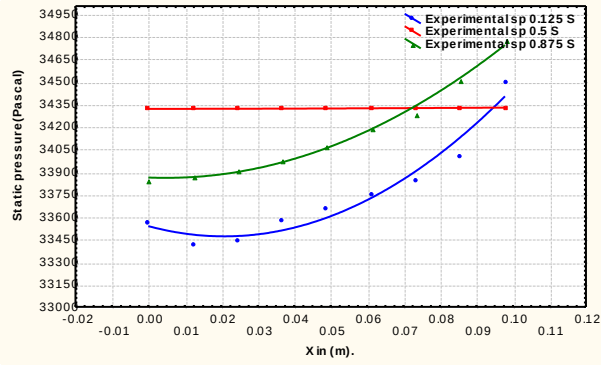

(e) For stagger angle=-12.

Fig.(15): Static pressure distribution for (0.125S, 0.5S and 0.875S).

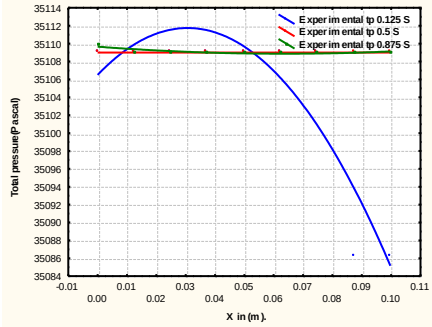

(a) For stagger angle=4.

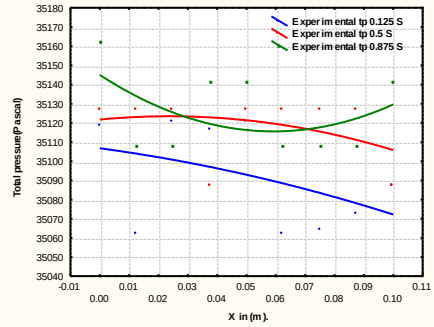

(b) For stagger angle=0.

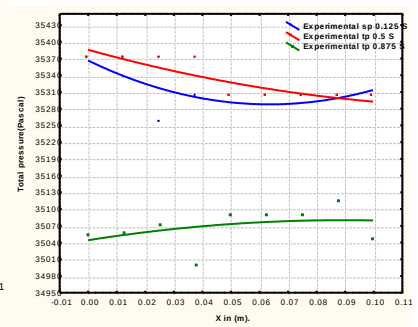

(c) For stagger angle=-4.

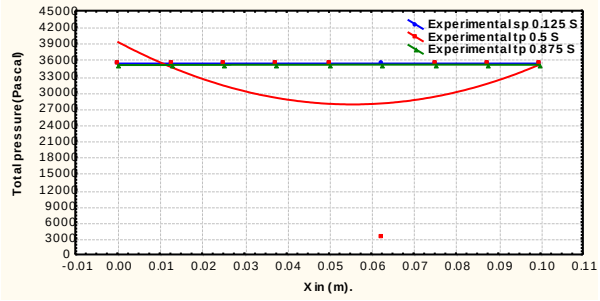

(d) For stagger angle=-8.

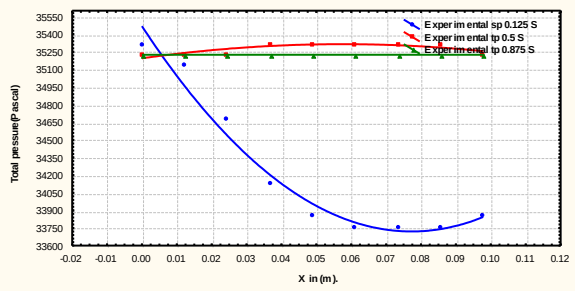

(e) For stagger angle=-12.

Fig.(16): Total pressure distribution for (0.125S, 0.5S and 0.875S).

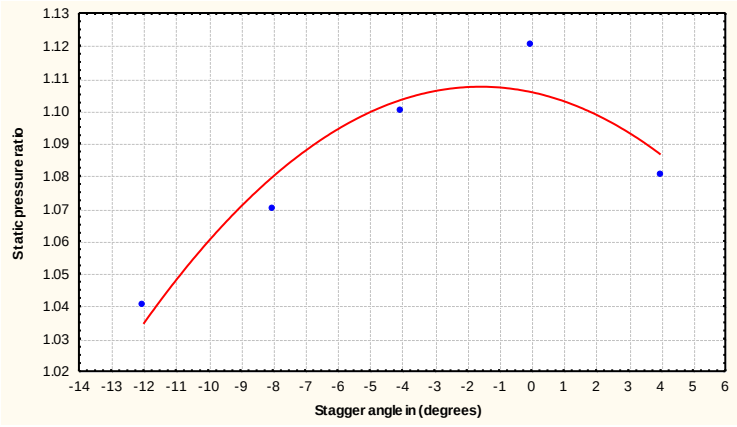

Fig.(17): Correlation of pressure ratio with stagger angles.

*** Smoke Tunnel Results:**

To see the real view and stream lines of flow separation on blade surface, the blade tests in smoke tunnel for stagger angle (4^0,0^0,-4^0,-8^0 and -12^0) are shown in fig.(18). The flow separation begins from the upper surface in stagger angle (-4^0).As the stagger angle increases, separation propagates towards the leading edge.

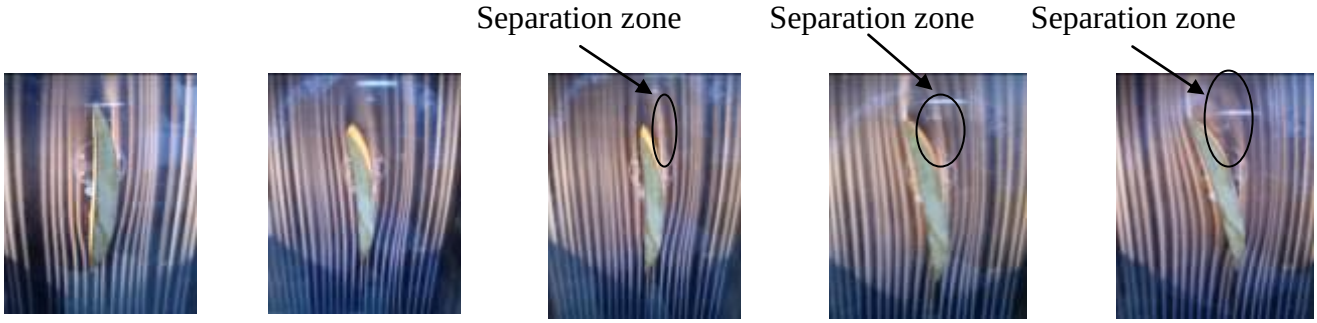

Fig.(18): Stream line distribution on surface of axial compressor blade section NACA 65_ (12)10: (A) Stagger angle =4. (B) Stagger angle =0. (C) Stagger angle =-4. (D) Stagger angle =-8. (E) Stagger angle =-12.

COMPUTATIONAL RESULTS:

The operating and boundary conditions for the flow passage between two axial compressor blades are listed in Table (3).

Table (3): Operating and Boundary Conditions.

Case	Stagger Angle in (degree)	Inlet Velocity (m/s)	Number of grid points	Number of iterations to convergence	CPU time in (min).
1	4	35	5473	8398	73
2	0	35	5573	7492	62
3	-4	35	5528	8403	74
4	-8	35	5440	8881	86
5	-12	35	4888	1019	93

The velocity and static pressure contours of flow between two axial compressor blades for stagger angles (4^0, 0^0,-4^0, -8^0 and -12^0) are presented in fig.(19) and (20). These figures show that the fluid flow being accelerated near and along suction side (upper surface of lower blade) up to a certain position, see the third column of tables (4). Then the flow decelerates to the exit for stagger angles (4^0 and 0^0) and to a certain position for stagger angles (-4^0, -8^0 and -12^0), see the

fourth column of table (4), where the flow separates from the blade surface. The flow decelerates near and along the pressure side (lower surface of upper blade) from the leading edge to the tailing edge along the chord line for all cases. The velocity and static pressure remains constant in the mid-space between the two blades from the inlet to the exit for stagger angles (-8^0 and -12^0) and to the certain position for stagger angles (4^0, 0^0 and -4^0), see the fifth column of tables (4). Then the flow decelerates to the exit. The fluid flow being accelerated as it passes through the contracting flow area after that the flow being decelerated to the trailing edge. These phenomena prove that the suction side works as a nozzle-diffuser, the pressure side works as a diffuser and the blade to blade configuration works as a nozzle-diffuser.

Table (4): Theoretical properties and behavior of flow between two blades in FLUENT.

No.	Stagger angles in (degrees)	Location of maximum velocity and minimum static pressure near and along the suction side (%chord)	Location of separation point near and along suction side (%chord)	Location of flow deceleration along mid-space between blades (0.5S)(%chord)
1	4	45	-	84
2	0	36	-	81
3	-4	35	98	74
4	-8	22	65	-
5	-12	12	63	-

The total pressure contours of flow between the two blades for stagger angle (4^0, 0^0,-4^0, -8^0 and -12^0) are presented in fig.(21) .This figure shows that the total pressure decreases as it passes from the inlet to the exit due to friction losses. The total pressure losses increases when the stagger angle increases (in clockwise direction) and the maximum total pressure losses occurs when stagger angle (-12^0) in separation region due to increased friction losses and adverse pressure gradient.

The flow separation affects the performance of a cascade and hence, affects the compressor performance where the pressure ratio decreases when the separation zone increases.

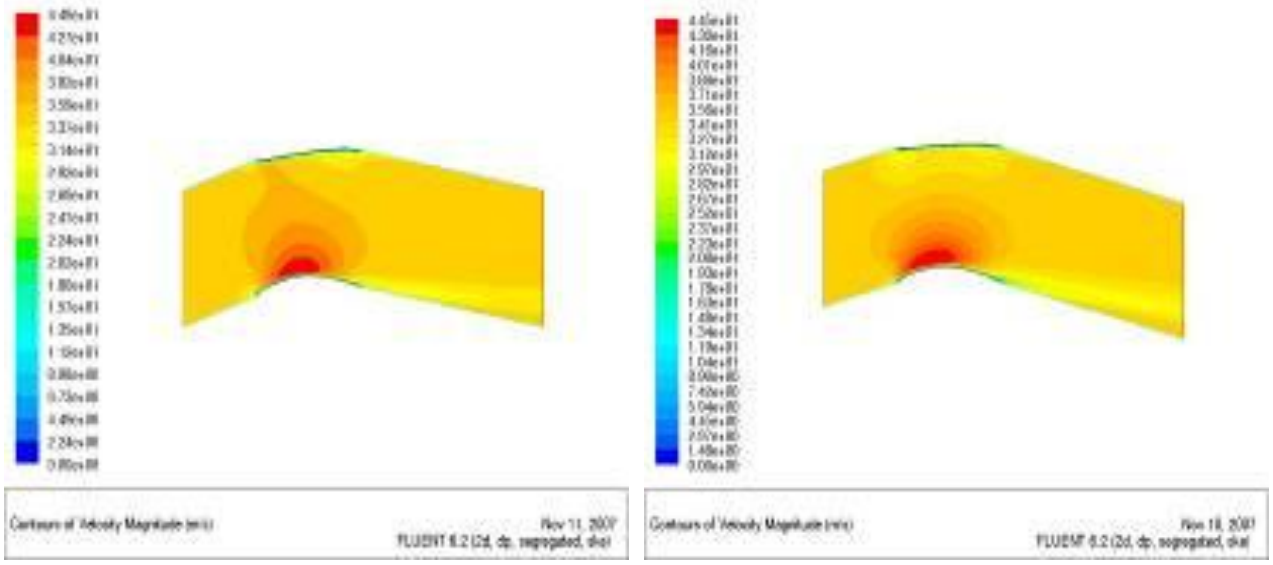

(a) (b)

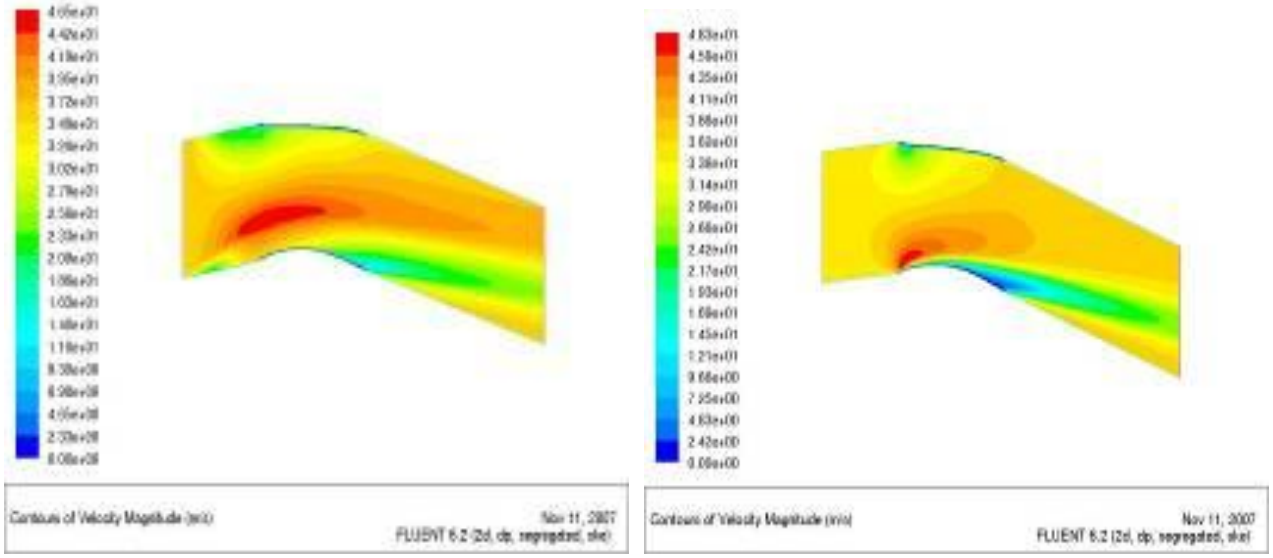

(c)

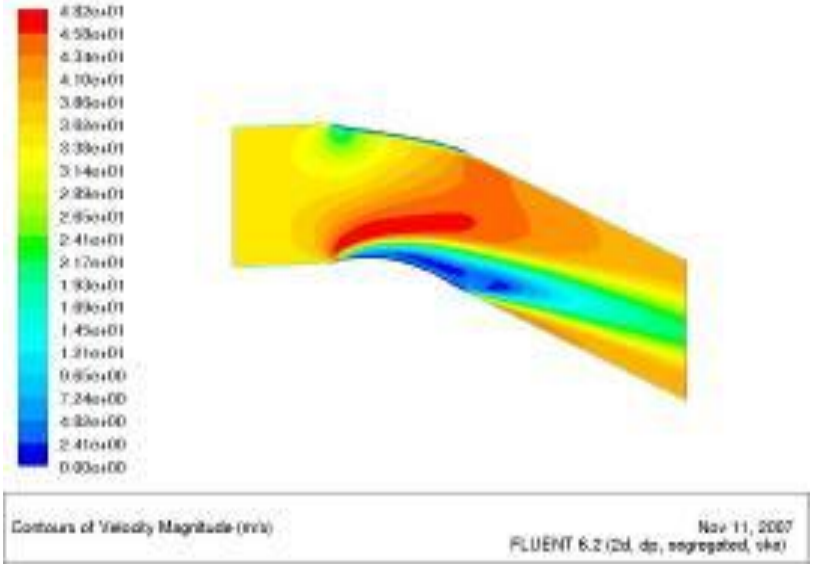

(e)

Fig.(19):Contours of velocity:(a) Stagger angle=4^0. (b) Stagger angle=0^0. (c) Stagger angle=-4^0. (d) Stagger angle=-8^0. (e) Stagger angle=-12^0.

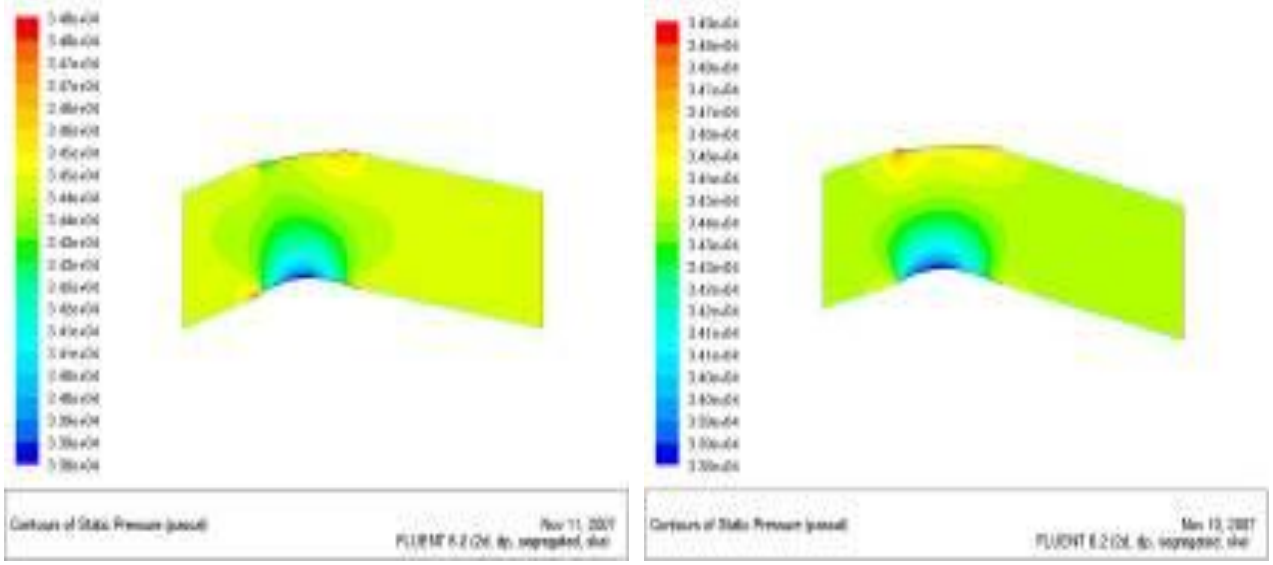

(a) (b)

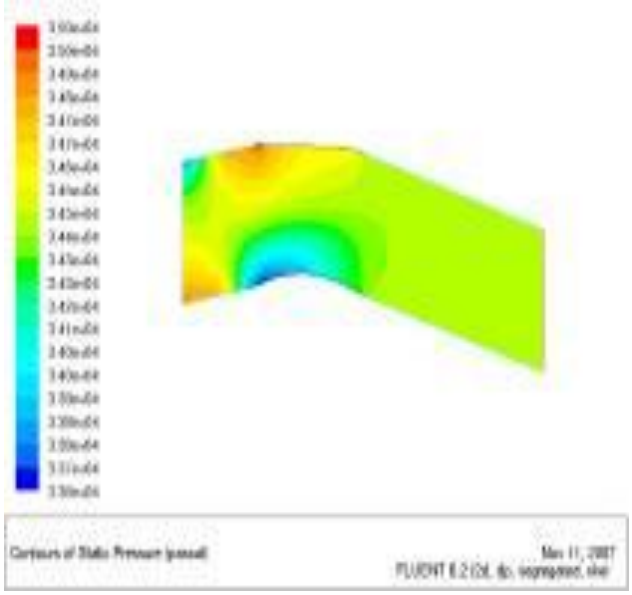

(c)

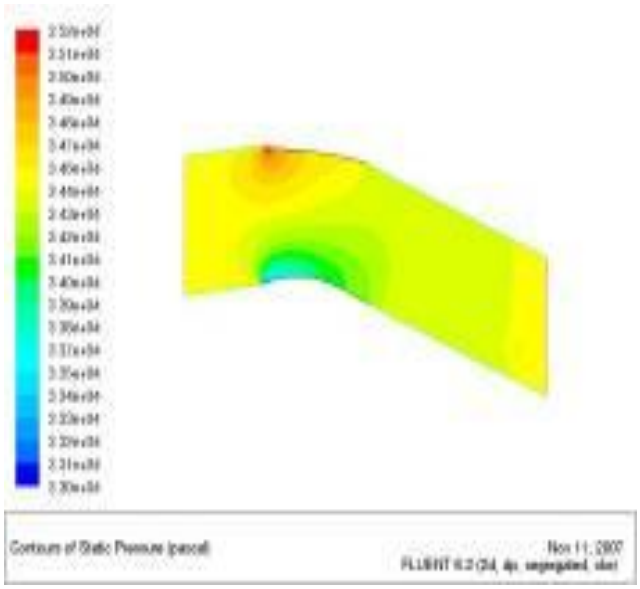

(d)

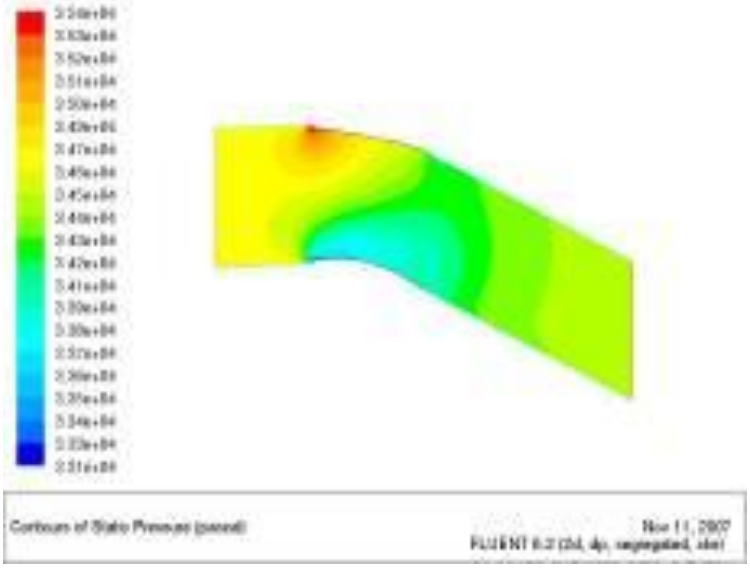

(e)

Fig.(20): Contours of static pressure: (a) Stagger angle=4^0. (b) Stagger angle=0^0. (c) Stagger angle=-4^0. (d) Stagger angle=-8^0. (e) Stagger angle=-12^0.

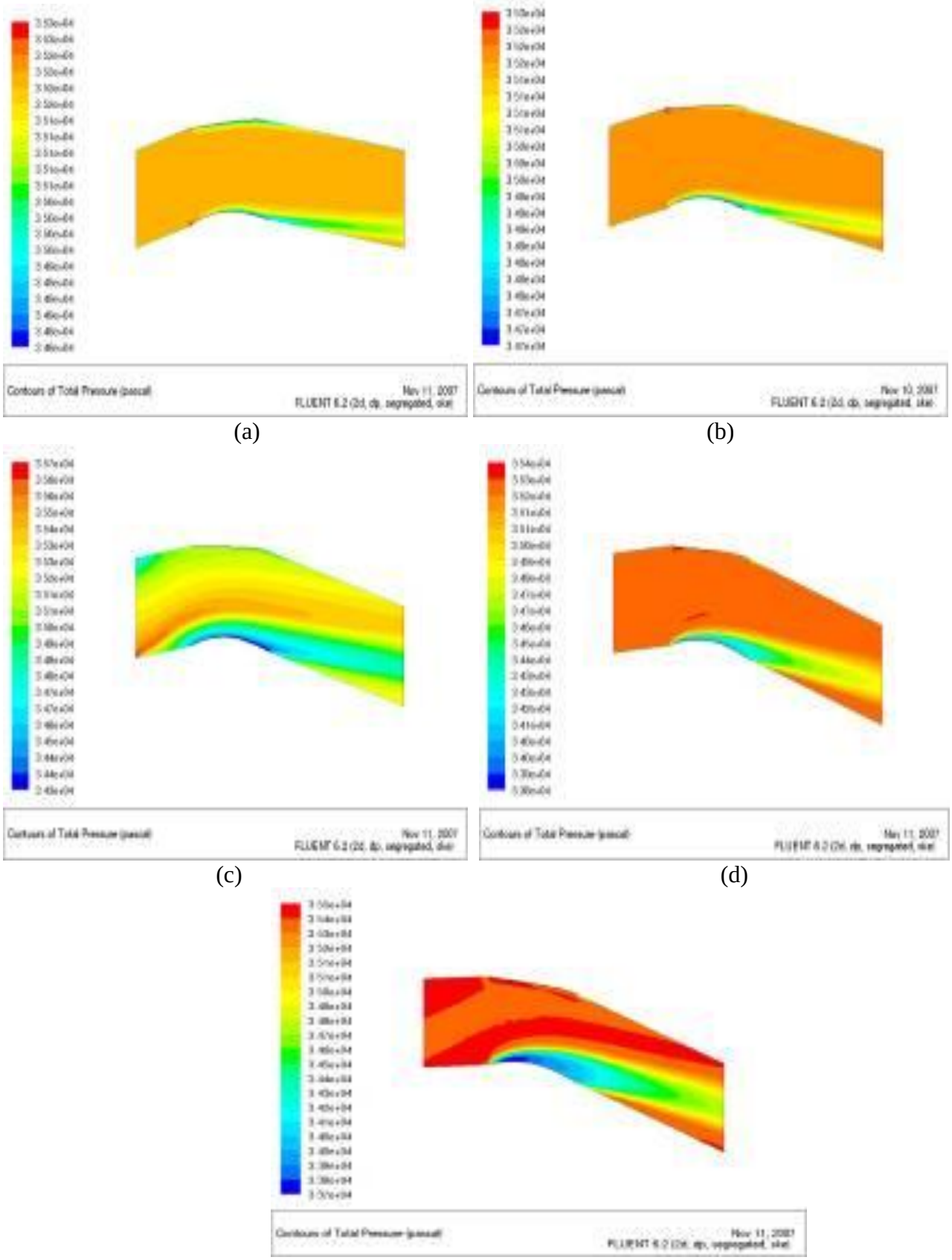

(a) (b)

(c) (d)

(e)

Fig.(21): Contours of total pressure: (a) For stagger angle=4^0. (b) For stagger angle=0^0. (c) For stagger angle=-4^0. (d) For stagger angle=-8^0. (e) For stagger angle=-12^0.

*** Accuracy of Solution:**

The FLUENT (V6.2) code is considered as a high accuracy computational fluid dynamics software package. Fig.(22) presents the distribution of residual and number of iterations for continuity, momentum and k-ε model equations and for stagger angle (0^0 and -8^0). As the stagger angle increases, the number of iterations to convergence increases because the problem gets complicated when the flow separation occurs, see table (3).

THE COMPARISON BETWEEN THE EXPERIMENTAL AND THEORICAL RESULTS:

The theoretical results obtained in this study by using FLUENT (V6.2) were compared with those obtained experimentally using the wind tunnel. Fig.(23) shows this comparison for the velocity in the three locations of interest for stagger angle (0^0).This figure shows good agreement between the theoretical and experimental results, where the flow behavior similar between these results and the range of different velocity between these results is(1-3)m/s.

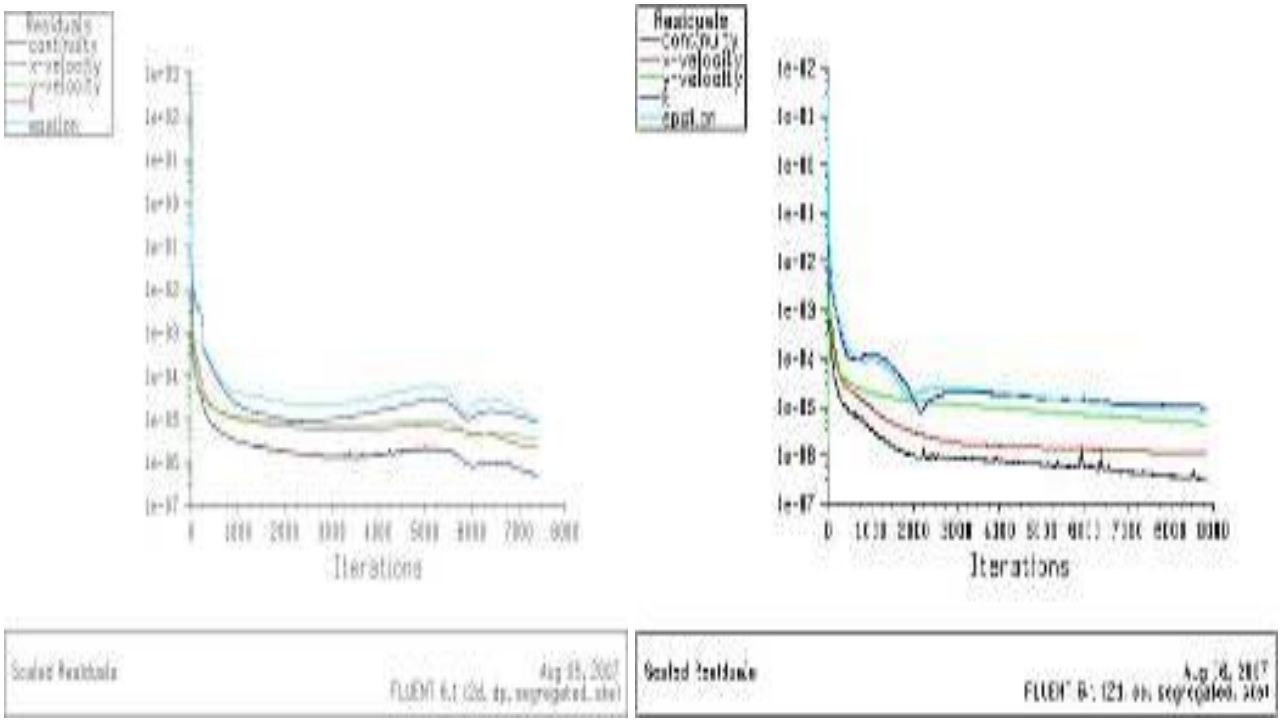

(a) For stagger angle=0. **(D)** For stagger angle=-8.

Fig.(22): Distribution of number of Iterations to convergence and Residuals for stagger angle (4^0 and -8^0)

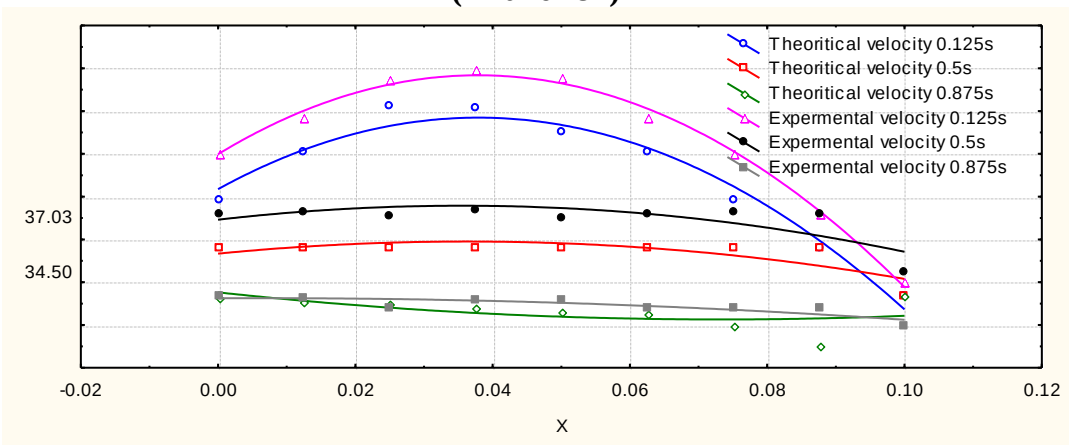

Fig.(23): The comparison of velocity distribution between the experimental results and the theoretical results.

CONCLUSIONS:

- 1-The area between two axial compressor blades for NACA 65_ (12)10 works as a nozzle-diffuser.
- 2-Smoke tunnel was successfully used to show separation of flow from upper blade surface.
- 3-The flow separation was seen to start at a stagger angle of (-4^0) experimentally and theoretically.
- 4- The mathematical relationship between the static pressure ratio and stagger angle for NACA 65_ (12)10 axial compressor cascade is concluded by using curve fitting method for polynomial distribution.

$$\frac{p_{s_e}}{p_{s_i}} = 1.1057 - 0.0021\theta - 0.0007\theta^2 \qquad \text{(n).}$$

The range of stagger angle for NACA 65_ (12) 10 axial compressor blade aerofoil is calculated from this relationship. It was found in the range (-18^0 to 36^0).

- 5- Total pressure was seen to reduce through the blade passage. It drops sharply for the separation zone.
- 6- FLUENT (V6.2) was used successfully to predict separation as compared to the experimental measurements in the wind tunnel and as compared with other works.

NOMENCLATURE

English Symbols

Symbol	Description	Units
C	Blade chord line.	m
C_1, C_2	Constants in turbulence model.	m
d, nd, zd	Dimension of pitot static tube.	m
E	Correction coefficient.	
E_0	Effect of static pressure holes distance.	-
G_k	Production term of kinetic energy.	kJ
g	Acceleration of gravity.	m/s^2
K	Kinetic energy of turbulence.	m^2/s^2
P	Pressure.	Pascal
n	Local coordinate normal to the wall.	m
Re	Reynolds number.	-
S	Space between two blades.	mm
x, y	Coordinates in X and Y- directions.	m
U	Velocity of air.	m/s
u, v, w	Velocity components in x, y and z directions	m/s

Greek Symbol

Symbol	Description	Units
α	Flow angle.	degree
β	Blade angle.	degree
ε	Dissipation rate of turbulent kinetic energy.	m^2/s^2
μ	Laminar viscosity.	kg/m.s
μ_e	Effective viscosity.	kg/m.s
μ_t	Turbulence viscosity.	kg/m.s

υ	Kinematic viscosity.	m^2/s
ω	Viscosity coefficients value.	-
θ	Stagger angle.	degree
ρ	Density.	kg/m^3
$\sigma_k, \sigma_\varepsilon$	Effective prandtl numbers.	-
Ω	Distance action from tube to wall.	-
$H\Delta$	Tube head in manometer.	o_2 cmH
$P\Delta$	Change in pressure.	Pascal

Superscripts

Symbol	Description
'	Fluctuating quantity.

Subscripts

Symbol	Description
air	Air.
d	Dynamic.
s	Static.
s_e	Static exit.
s_i	Static inlet.
t	Total.
water	Water.
1	Inlet conditions.
2	Outlet conditions.

Abbreviations

Symbol	Description
A.C motor	Alternating Current Motor.
CFD	Computational Fluid Dynamics.
Fig.	Figure.
NACA	National Advisory Committee for Aeronautics.
NASA	National Aeronautics and Space Administration.
SIMPLE	Simi – implicit method for pressure linked equations.
SIMPLEST	SIMPLE – Specially Treated (Newly developed).

REFERENCES

- Chittiappa Muthanna, "Flow field Downstream of a Compressor Cascade with Tip Leakage", Ph.D. thesis, Virginia Polytechnic Institute and State University, Aerospace Engineering Department, November, 1998.

- Hill, P. G., and Peterson, C. R., "Mechanics and thermodynamics of propulsion", Addison-Wesley publishing Company, Inc. 1965.

- Jones, W. P. and Launder, B. E., "The Predication of Laminariztion With a Two-Equation Model of Turbulence", Journal of Heat and Mass Transfer, Vol.15, pp.301-314, 1972.

- Meinhard T. Schobeiri, Burak Öztürk and David E. Ashpis, "On the Physics of Flow Separation A long a Low Pressure Turbine Blade Under Unsteady Flow Conditions", Texas A&M University, Turbomachinery Performance and Flow Research Laboratory, College Station, Texas 77843, Available from: NASA Center for Aerospace Information 7121 Standard Drive Hanover, MD 21076, http://gltrs.grc.nasa.gov and National Technical Information Service 5285 Port Royal Road Springfield, VA 22100,June, 2003.

- Moult, A., and Srivatsa, S. K.,"CORA-2 A computer program Code for Axi-Symmetrical Combustion chambers", CHAM Computer Code 201, 1977.

- Omran, K. J., "An Experimental Study of Backward Facing Step's Effect on The Aerodynamic Characteristics of Airfoil at Low Flight Speeds", M.Sc. Thesis, Aeronautical Specialization, Department of Machines and equipments, University of Technology, 2003

- You D. AND Moin, P., "Large-eddy simulation of flow separation over an airfoil with synthetic jet control", Center for Turbulence Research, Annual Research Briefs, 2006.